JAIEP

A Predictive Model for Climate Change Using Advanced Machine Learning Algorithms in Egypt

Yasmeen Ali Shalaby [1*], Asmaa Saeed Embark [2]

[1] Business Information System, El Gazeera High Institute For Computer & Management Information System, Cairo 11518, Egypt; dr.shalaby.yasmeen@gmail.com

2 Business Information System, El Gazeera High Institute For Computer & Management Information System, Cairo 11518, Egypt; asmaasaeed20104@gmail.com

* Corresponding author: dr.shalaby.yasmeen@gmail.com, dr.yasmeen@commerce.helwan.edu.eg

Abstract

This study evaluates advanced machine learning (ML) models for forecasting daily average temperatures in Egypt, using a dataset from one of the world's most climate databases, the GHCN-D of the NCEI under NOAA (United States). The dataset spans nine years (January 1, 2015 - December 31, 2023) and consists of 73,562 daily records from 23 climate stations across Egypt, covering eight climate features. A comparative analysis was conducted between LSTM networks and other algorithms, involving XGBoost, Random Forest, Gradient Boosting, Support Vector Regression, ARIMA, and Linear Regression. The LSTM model represented clear superiority achieving $R^2 = 0.97$, MAE = 0.07 °C, and MSE = 0.01 °C², strongly outperforming all other models, specifically in capturing long-term temporal dependencies in time series of climate. The study forecasted Egypt's daily average temperature for August 2025. The results present a steady upward trend from about 33°C on August 1 to around 34.4°C on August 29. This gradual height aligns with peak summer in Egypt's desert climate, which may indicate seasonal broader climate variance influences, consistent with the previous predictions of increasing temperatures. The results confirm that deep learning, specifically LSTM, presents improvements over traditional methods for temperature forecasting, providing a highly accurate predictive model. Our research contributes to advancing climate change capabilities in Mediterranean and dry regions, with practical influence for agricultural planning, environmental monitoring, and climate adaptation.

Keywords: Prediction, machine learning, regression, climate change, Egypt.
MSC: 60G25; 86A08

Doi : https://doi.org/10.21608/jaiep.2025.415474.1020
Received: August 19, 2025, Revised: October 4, 2025, Accepted: October 5, 2025

1. Introduction

Climate change significantly affects plant growth, food production, sustainable economic development, and people's health. With the increasing availability of comprehensive historical climate data and the growing demand for accurate production prediction, there is a pressing need for reliable methods to identify the stochastic relationship between past and future values. Accurate temperature forecasting plays a crucial role in climate change risk

management, as it supports early warning systems and mitigates the adverse impacts of weather events, like heat, droughts, heavy rainfall, and cold spells [8]. Thus, developing forecasting accuracy has become a priority for enhancing both scientific understanding [1].

Recent advances in numerical weather prediction models and observational technologies, involving meteorological satellites, have significantly increased the accuracy of temperature forecasting at various spatial and temporal regions [6]. Statistical models often rely on simplified assumptions regarding data distribution [18]. Advanced ML approaches have gained importance in recent years. Especially deep learning DL techniques have shown strong potential in capturing high-dimensional, nonlinear, and dynamic meteorological data, enabling more adaptive predicting outcomes [4]. Machine learning techniques, such as CNNs and hybrid CNN-LSTM models, have shown remarkable progress in predicting extreme climate events [10]. These models address the limitations of traditional methods by handling long-term dependencies and nonlinear relationships, offering superior accuracy for predicting temperature, precipitation [10]. Also, ML applications extend to climate mitigation areas like optimising transportation and energy systems, as well as adaptation strategies such as improving disaster management [16]. However, challenges remain, involving the computational intensity of models and their reliance on huge datasets [15]. The scarcity of reliable observational data for past extreme events further complicates forecasting, often requiring ensembles of dynamic models that may misinterpret drivers due to model limitations [15].

Advanced computational methods are vital for capturing climate impacts. Ibrahim et al. (2021) [13] used ML with satellite data for climate change in North-East Africa, while Shams et al. (2023) [17] developed machine learning based temperature forecasting models under climate change effects, supporting capabilities to address climate change in agriculture challenges. ML presents promise for water resource management. Elbeltagi et al. (2023) [9] employed ML and best subset regression to predict daily reference evapotranspiration in Egypt, aiding irrigation planning and water optimisation. Also, machine learning combined with remote sensing revolutionises environmental monitoring. Vulova et al. (2021) [20] integrated remote sensing, flux footprints, and AI to effectively model urban evapotranspiration, yielding agriculturally relevant insights for water management and climate analysis. Hybrid approaches combining multiple ML techniques with economic analysis significantly enhance forecasting accuracy and present insights for agricultural and policy planning, addressing the complex interplay of environmental and economic factors [2]. Despite these advances, challenges remain in integrating diverse data sources, capturing temporal dependencies, which require further research.

Traditional econometric methods, like linear regression and time series analysis, have been widely used for agricultural cost forecasting [14]. However, these methods struggle to monitor the complex interactions and non-linear relationships between different environmental factors [7]. Time series models, like ARIMA, are applied to agricultural price forecasting but often fail to incorporate exogenous variables like environmental features, limiting their precision and applicability to dynamic farm systems [19]. ML techniques, including tree-based models and DL, have emerged as more efficient alternatives. RF and DT have been used for forecasting agricultural production costs and presented predictive capabilities when managing diverse input factors [3]. Even so, Deep learning approaches, such as LSTM networks, have shown in addressing these limitations by monitoring long-term dependencies in time-series data and improving prediction accuracy [11]. Despite their success, these methods can be computationally dense and may require huge datasets to achieve optimal coefficients.

2. Related work

Temperature prediction in Egypt is a main issue in addressing climate change, due to its direct impact on water resources management, agriculture, and public health. Research has shown that ML techniques can monitor complex climatic patterns and achieve forecast accuracy that surpasses traditional approaches. Houssein et al. (2025) [12] introduce the

proposed approach is a deep long short-term memory model using genetic algorithms and the mountain gazelle optimiser, which collectively fine-tune the architecture of the DLSTM model. It used historical climate data from nine Egyptian cities: Dakhalia, Bane-Suef, Aswan, Behira, Menoufia, Minia, Sharkia, Qalyubia and Sohag to estimate the model's performance. The effectiveness of the MGO-GA-DLSTM model was compared with other forecasting models. The results demonstrate that the MGO-GA-DLSTM model outperforms existing methods in climate forecasting, offering improved accuracy.

Berk, et al., (2025) [5], used Gradient Boosting to forecast the air temperature and the Steadman Heat Index. Paris, France, during the late summer and spring months, is the focus. The years 2018 through 2024. The data are curated as a multiple time series for each year. Predictors involve seven collected indicators of weather. Predicting uncertainty is addressed with conformal prediction areas. Cairo, Egypt, is a second location using data over the same years and months. Cairo is a more challenging setting for temperature prediction because its desert climate can build abrupt and erratic temperature variance. However, there is some progress in predicting hot days. Vulova et al. (2021) [20] improved a model for estimating urban evapotranspiration by combining remote sensing data with flux footprints and AI. Using 2018–2020 datasets from urban areas in Germany, they compared an Artificial Neural Network incorporating flux footprint data with a satellite-only model. achieving $R^2 = 0.91$ versus $R^2 = 0.79$.

Similarly, Barakat et al. (2025) [2] created a hybrid ML to predict agricultural production costs in Egypt by integrating environmental analysis with sensitivity assessments to climate variables. Using 2010–2023 data that involved economic indicators such as input prices, production costs and climate variables like temperature and precipitation, they combined (RF) with Multiple Regression. This hybrid method achieved $R^2 = 0.89$, MR alone ($R^2 = 0.77$), demonstrating its reliability for agricultural planning under economic and climate uncertainty.

Elbeltagi et al. (2023) [9] developed forecasting models for daily reference evapotranspiration in key Egyptian locations using 1980–2020 climate data. Comparing Best Subset Regression, RF, and ANNs, they found ANNs achieved the highest accuracy ($R^2 = 0.94$, RMSE = 0.21) versus BSR's RMSE of 0.26, confirming ANNs' superiority for accuracy in agriculture and water management in arid regions. Ibrahim et al. (2021) [13] used an RF algorithm to detect climate change signals in Northeast Africa with 2000–2020 satellite-based temperature and precipitation data. By combining spatial and temporal datasets, they improved the model efficiency to $R^2 = 0.87$, the spatial-only model ($R^2 = 0.81$), presenting the value of temporal data combining for large-scale climate change monitoring. Shams et al. (2023) [17] developed an advanced ML-based modeling specifically designed to predict temperature patterns across Egypt, using climatic datasets spanning 35 years (1985 -2020) to ensure temporal coverage and reliable pattern identification, implementing a comparative analysis between present Linear Regression, Random Forest regressor, Decision Tree regressor, (KNN) regressor, (SVM) regressor, and Cat Boost Regressor as machine learning regressors. The results indicated that CBR achieved increased results compared to the recent machine learning techniques. The evaluation of the proposed model investigated that the CBR achieved (MSE), (RMSE), (MAE), and the determination Coefficient R2 are 0.003, 0.054, 0.0036, and 92.40%, respectively.

3. Objectives

The primary objective of this research is to evaluate ML models for accurately forecasting daily TAVG over a nine-year historical period, with a focus on comparing deep learning approaches, specifically Long Short-Term Memory networks, with other algorithms such as XGBoost, RF, GB, SVR, ARIMA, and LR. This study aims to determine the most efficient predictive methodology for monitoring long-term temporal dependencies and minimizing predicting errors, thus enhancing climate forecasting accuracy.

4. Research Gap

Doi : https://doi.org/10.21608/jaiep.2025.415474.1020
Received: August 19, 2025 Accepted: October 5, 2025

Despite the research on climate change prediction using ML in Egypt, important gaps remain, involving the scarcity of long-term forecasting models that account for climate variance scenarios extending to 2050 or 2100, the absence of studies combining global climate models with ML algorithms at the local level, the limited incorporation of real-time data in predictive models, which hampers the accuracy of urgent decision-making, and the insufficient integrated spatial-temporal analysis, especially when integrating satellite imagery with long-term time-series data.

5. Methodology

Figure 1 presents the methodological model to process and analyze climate change in Egypt from 2015 to 2023 over 9 years, aiming to build an accurate predictive model using regression technique algorithms. The research followed an approach, beginning with data collection from sources, followed by data cleaning and processing to determine and address missing values. The data was then transformed into formats suitable for machine learning.

The researchers used a set of statistical models and advanced ML algorithms such as LSTM, XGBoost, and RF. The efficiency of each model was estimated using standard metrics (MAE, MSE, R^2) to measure prediction accuracy. The experimental analysis ensured fair comparisons via models by splitting the data into training and test sets using methods compatible with the temporal data. This methodology presents a practical model for future applications, like early warning systems, enhancing the understanding of climate change in Egypt, and supporting decision-making in the agricultural and environmental sectors.

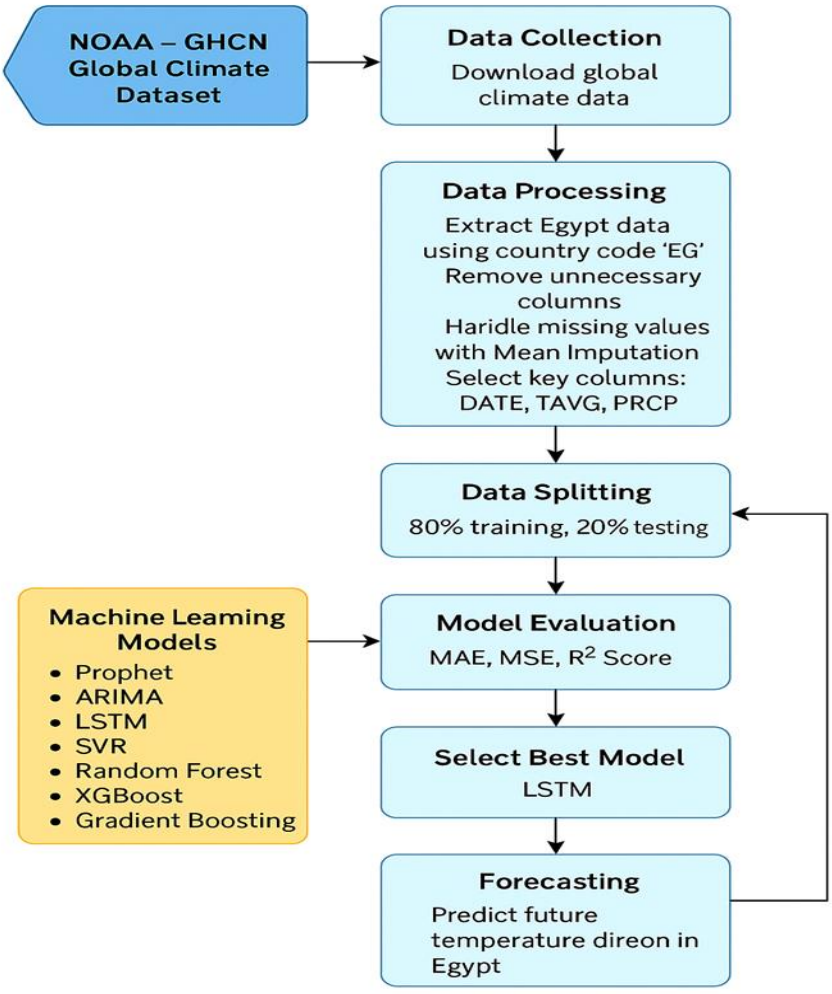

Figure 1: model for predictive temperature with machine learning.

5.1 Dataset Description

This paper relied on precise climate data obtained from one of the world's most comprehensive databases, the National Centers for Environmental Information (NCEI) under the National Oceanic and Atmospheric Administration (NOAA) in the United States. The data was specifically extracted from the Global Historical Climatology Network Daily (GHCN-D), which presents reliable climate data from thousands of ground-based monitoring stations worldwide.

The data covers 9 years, from 1 January 2015 to 31 December 2023. Annual data files in CSV format were downloaded and merged utilizing advanced tools such as Google Colab and Python to ensure consistency. Since the research focuses on a specific region, the dataset was filtered to extract only the readings recorded by climate monitoring stations in Egypt, determined by the country code EG. This resulted in 73,563 rows representing daily records of different climate features. After completing the processing stages, the final dataset was ready for analysis, containing 73,562 climate readings distributed by 8 different climate variables, including 23 climate stations in Egypt determined from NOAA's database. This provides a robust and informative foundation for the study.

A comprehensive list of the 23 GHCND stations utilized in this analysis, including their IDs, names, data coverage, geographic coordinates, and rates of missing data, is provided in Appendix C.

5.2 Key Variables in the Dataset:

A singular national daily average temperature series was created by consolidating records from the 23 GHCN-D stations for the national aggregation of station data. The aggregate was conducted as an unweighted arithmetic mean over all accessible stations daily. In instances of absent data from a station on a specific day, the mean was computed utilizing the data from the other stations. This method guarantees a uniform national signal while reducing the impact of localized deficiencies. Table 1 presents the primary columns and variables in dataset.

Table 1: Description of dataset.

Variable Name	Description
station	Monitoring station code
date	Date of the recorded observation (format: YYYYMMDD)
element	Type of climate variable (e.g., TMAX, TMIN, PRCP, SNOW, TAVG)
value	Measured value of the specified element (originally stored in tenths of °C; converted to °C for TMAX, TMIN, and TAVG)
time	Time of observation (e.g., hour of the day, may be missing in some records)
PRCP	Precipitation amount (tenths of millimeters)
TMAX	Maximum temperature of the day (tenths of °C)
TMIN	Minimum temperature of the day (tenths of °C)
SNOW	Snowfall amount (tenths of millimeters, typically 0 for Egypt)
TAVG	Average temperature of the day (tenths of °C, not always available)

Doi : https://doi.org/10.21608/jaiep.2025.415474.1020
Received: August 19, 2025 Accepted: October 5, 2025

5.3 Data Preprocessing

Several stages were implemented to process and refine the data before its use in the models, as follows:

5.3.1 Data Merging

All station-specific files for Egypt were combined into a single comprehensive CSV file.

5.3.2 Variable Selection

Conversion of Units: The GHCN-D dataset documents temperature measurements (TMAX, TMIN, TAVG) in tenths of degrees Celsius. Prior to executing any data cleaning, imputation, statistical analysis, model training, or visualization, all temperature variables were standardized to °C by dividing the raw values by 10.

For instance:

$$\frac{{}_{\text{raw}}T}{10} = {}_{\text{C}}T \tag{1}$$

After this stage, the study uniformly presents temperatures in °C (and °C² for squared-error measures) throughout all tables, figures, and evaluation metrics (MAE, MSE, R^2).

The following variables were used in the models:

Table 2: Description of Dataset Variables

Variable Name	Description
DATE	Daily recording date
TAVG	Daily average temperature (°C), converted from GHCN tenths
PRCP	Daily precipitation amount (millimeters)
STATION	Monitoring station code
ID	Combined country and station identifier (e.g., EG000062304)

5.3.3 Data Cleaning

Unnecessary columns were excluded; The DATE column was converted to DATETIME format. Finally, the data was sorted chronologically.

5.3.4 Handling Missing Values

Mean Imputation was utilised, where missing values in columns were filled using the mean of each column. Missing values were computed using the mean of each variable, computed strictly within the training split to avoid any information leakage from the test set. Specifically, for each feature (TAVG, TMAX, TMIN, PRCP), the mean was calculated using only the training portion of the data (2015–2021) and then applied to both the training and test periods. This ensured that the test set remained unseen and independent during model evaluation.

Treatment of missing TAVG values. In cases where the daily average temperature (TAVG) was not available in the GHCN-D records, it was inferred as the arithmetic mean of the corresponding TMAX and TMIN values, following the NOAA convention:

$$\frac{TMAX + TMIN}{2} = TAVG \quad (2)$$

This rule was applied only when both TMAX and TMIN were present, which covered approximately 4.5% of the missing TAVG entries. Days with incomplete TMAX or TMIN records were excluded from the analysis.

5.3.5 Quality Verification

Checks were performed to confirm that no duplicate values or overlapping dates existed. After cleaning, the data was ensured to be ready for use in models.

5.3.6 Time Series Analysis

The aim was to observe temperature trends in Egypt (2015 to 2023). By two steps, A Table was created to structure each row as a day with values for each feature: TMAX, TMIN, and TAVG. Then, the evolution of the average temperature TAVG over the years was plotted.

All temperature values shown in the following figures are expressed in °C after conversion from GHCN tenths.

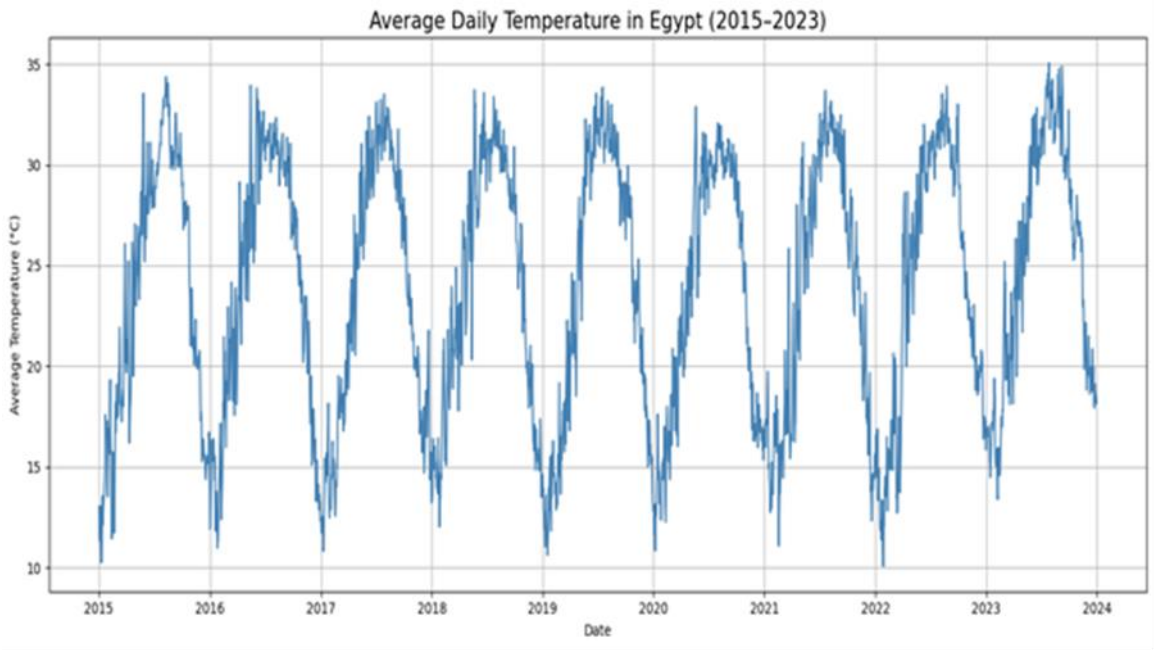

Figure 2: average daily temperature in Egypt (2015-2023).

Figure 2 shows the change in daily average temperatures in Egypt (2015 to 2023), helping to determine general trends of increase or decrease over time, higher temperatures in summer and lower temperatures in winter. The X-axis represents dates in a specific period. The y-axis represents average temperature in Celsius (°C). The Blue Line represents the change in daily average temperature over time.

6. Analysis and Visualization of Maximum (TMAX) and Minimum (TMIN) Temperatures

Doi : https://doi.org/10.21608/jaiep.2025.415474.1020
Received: August 19, 2025 Accepted: October 5, 2025

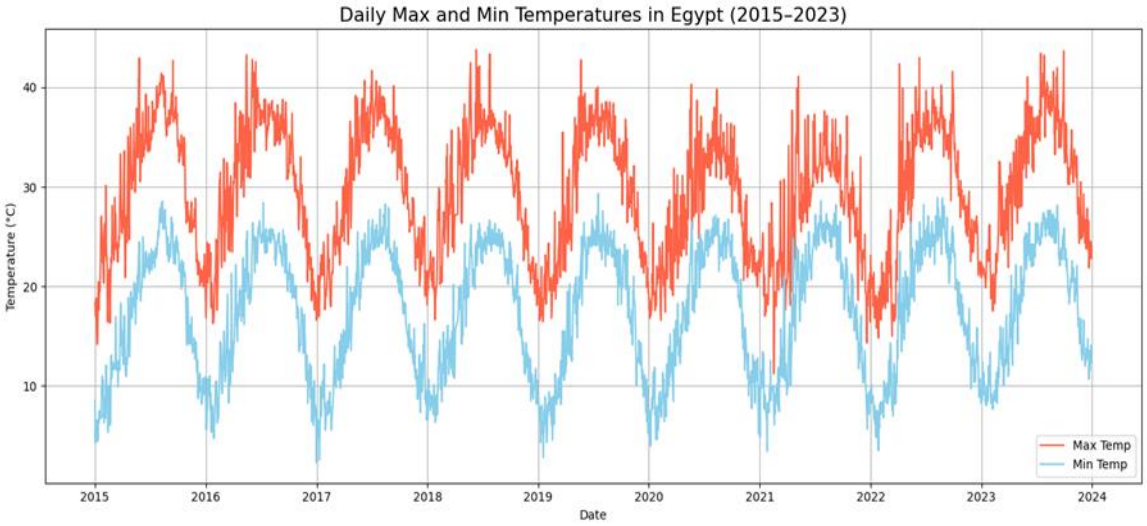

Figure 3: daily max and min temperatures in Egypt (2015 – 2023)

Figure 3 presents the daily maximum and minimum temperatures in Egypt (2015 to 2023), represented as a time series. The red line fluctuates between 25°C and 40°C, peaking in summer months mid-year 2015, 2016, etc., while the blue line varies between 5°C and 25°C, dipping in winter periods. The seasonal pattern is evident, with increasing temperatures in summer and decreasing temperatures in winter across all years. The overall trend suggests stable climatic conditions, though short-term variability is visible within each year.

7. Statistical Distribution Analysis of Temperatures

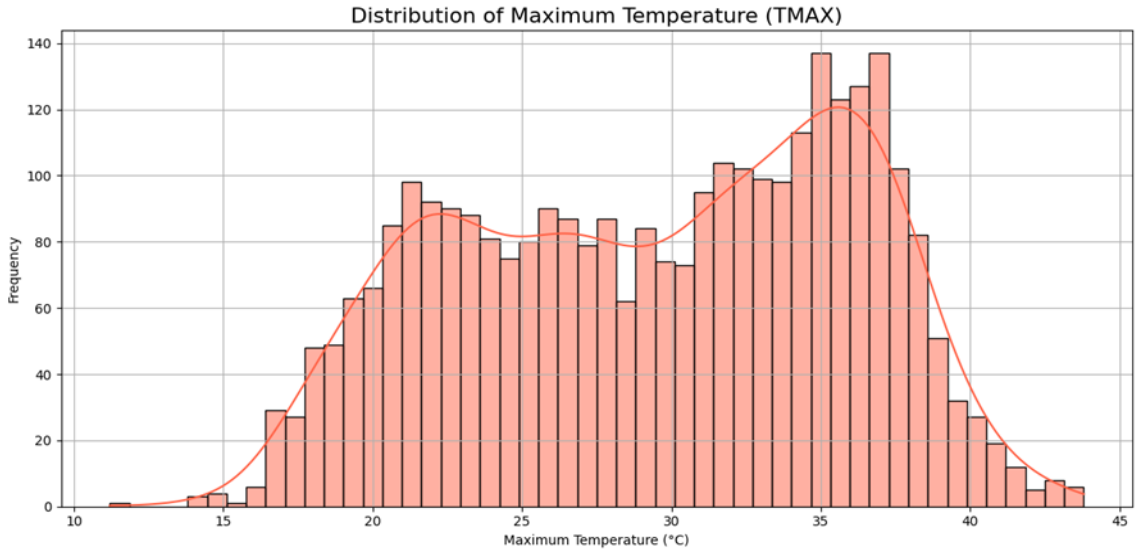

Figure 4: Distribution of Maximum Temperature (TMAX):

Figure 4 illustrates the distribution of maximum temperature in degrees Celsius (°C). The vertical axis reflects the number of occurrences for each temperature category. The figure presents a bell-shaped distribution with a peak frequency around 30°C to 35°C, where the highest columns reach approximately 120-140 occurrences, indicating this range as the most common TMAX. The distribution is a symmetrical normal distribution, with frequencies decreasing on both sides, lower frequencies below 20°C and above 40°C, with minimal occurrences near the extremes, e.g., 10°C and 45°C. A symmetrical pattern, indicating that the data follows a unimodal distribution centered around the 30-35°C range, which is typical for areas with a warm climate through the monitoring period, such as summer months.

8. Distribution of Minimum Temperature (TMIN):

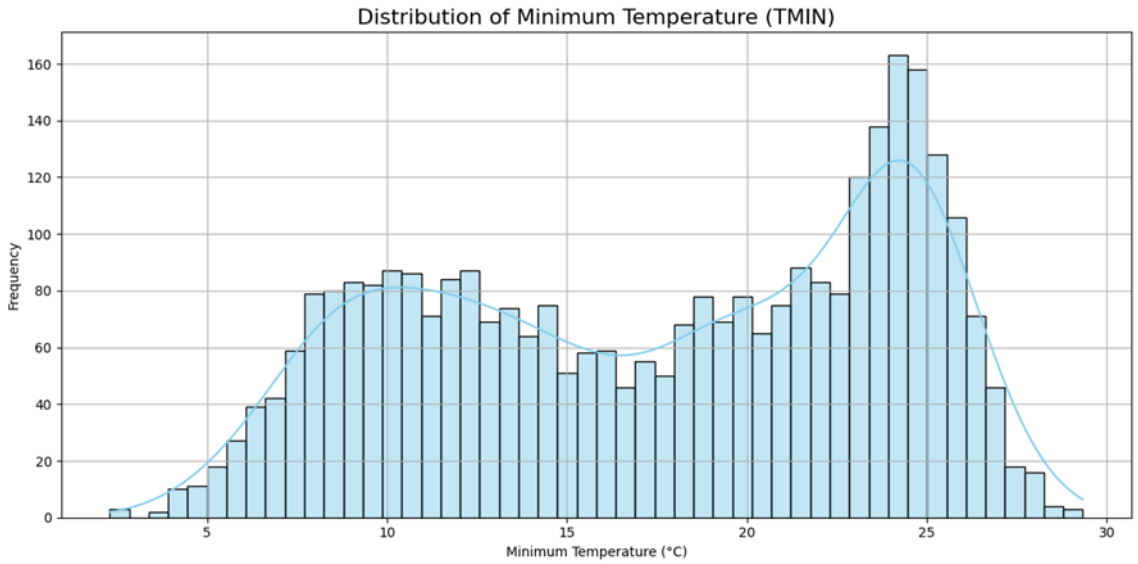

Figure 5: Distribution of Minimum Temperature (TMIN)

Figure 5 shows the statistical distribution of minimum temperatures in Egypt, highlighting a concentration of values within moderate temperature ranges, along with the occurrence of some extremely cold days, particularly during the winter season. The vertical axis presents the number of days on which a minimum temperature was recorded. The data are displayed as a frequency distribution of temperatures, while the blue line over the columns depicts the Kernel Density Estimate (KDE), representing the overall probabilistic distribution of temperature values. This frequency distribution and KDE enable a more understanding of the spread of minimum temperatures, indicating the most common values and their different range, thereby assisting in the analysis of climatic patterns.

9. Distribution of Average Temperature (TAVG):

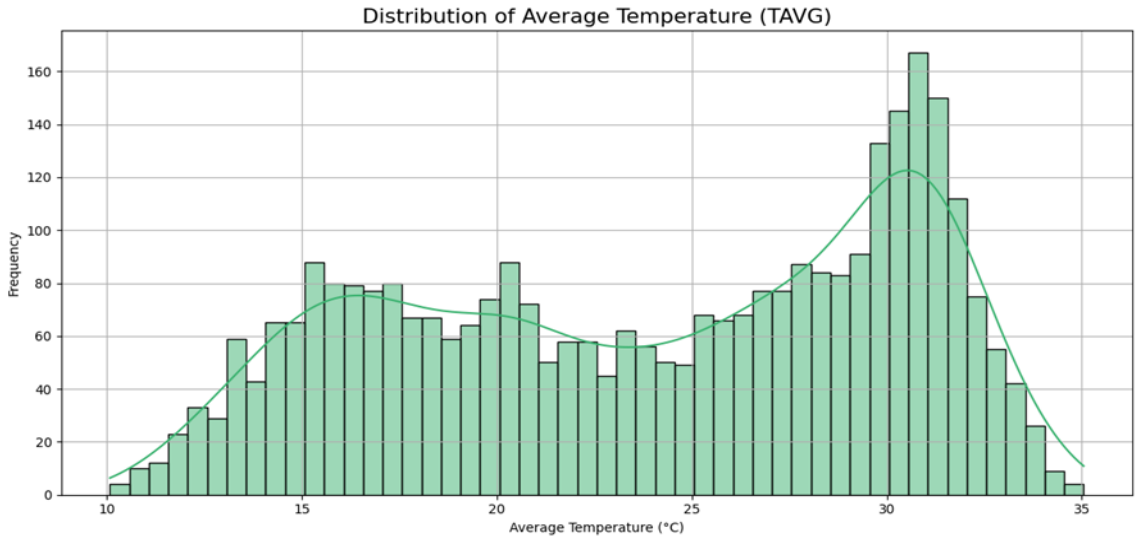

Figure 6: Distribution of Average Temperature (TAVG)

Figure 6 presents the statistical distribution of average temperatures in Egypt, an effective tool for determine months with moderate or hot climates. The data are displayed as the frequency distribution of temperatures within defined thermal bins, while the line above the columns depicts the KDE, which provides the overall probabilistic distribution of

Doi : https://doi.org/10.21608/jaiep.2025.415474.1020
Received: August 19, 2025 Accepted: October 5, 2025

temperature. This combination of frequency distribution and KDE present an understanding of the average temperature distribution patterns, thereby contributing to the evaluation of climatic features and the identification of periods with moderate or hot weather conditions within the study period.

10. Distribution of Precipitation (PRCP):

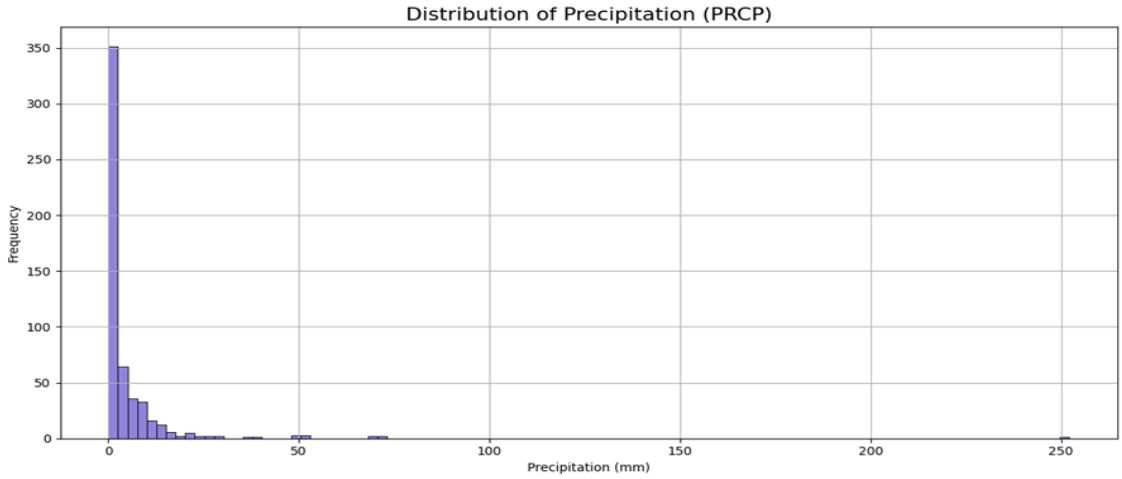

Figure 7: distribution of precipitation (PRCP)

figure 7 presents the distribution of precipitation (PRCP) meaning distribution of precipitation amounts in millimetres, with the horizontal axis from 0 to 250 mm in regular intervals, and the vertical axis providing frequency from 0 to 350 for the number of observations per category, indicating a positively skewed distribution with a high peak at 0 mm (about 340 occurrences) indicating dry days and minimal precipitation, followed by a sharp low in frequency as precipitation increases (50-100 at 0-10 mm, and less than 10 above 50 mm), reflecting the prevalence of light rains and the rarity of floods, with significant different supporting climate analysis and modelling using distributions like gamma.

11. Monthly Average of Temperature (TAVG) and Precipitation (PRCP) in Egypt (2015–2023):

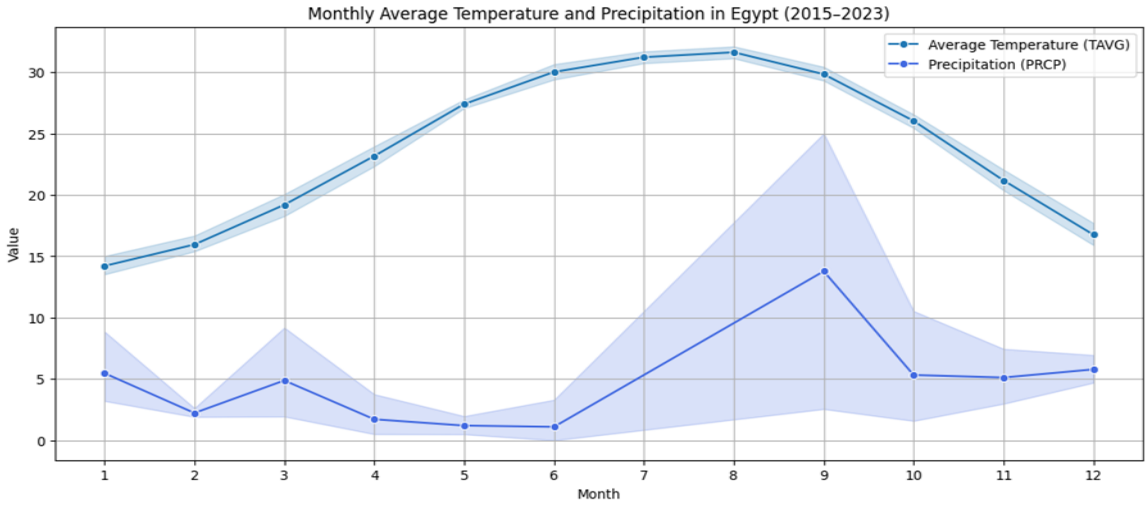

Figure 8: Monthly Average of Temperature (TAVG) and Precipitation (PRCP).

Figure 8 presents the monthly averages of temperature in dark blue and PRCP in light blue with shading in Egypt. The TAVG line starts at about 13–15°C in January, rises to its peak of 28–30°C in July and August, then reduction to 15°C in December, which reflects the seasonal cycle of a hot climate, with an annual average of about 20–22°C and a seasonal range

reaching 15°C. The PRCP line presents very low precipitation, less than 10 mm, with two peaks in winter (December–February: 5–10 mm) because of Mediterranean storms, and a drop to near zero in summer (June–August) under the influence of high-pressure systems. This ensures an extremely arid climate with an annual average below 50 mm, an inverse relationship between temperature and precipitation, supporting climate change research and environmental risk, such as drought evaluation, despite limitations such as the lack of influence of anomalous years.

12. Data Splitting

The dataset was temporally split into 80% training to learn historical patterns and 20% testing, confirming that the temporal sequence was preserved without randomization. Seven models, combining statistical methods, ML algorithms, and neural networks, as shown in Table 3, using regression techniques through the scope of time series forecasting, were employed for climate data analysis: ARIMA, LSTM, RF, XGBoost, GBR, SVR, and LR. This set of models enables an evaluation of predictive effectiveness via different methods for forecasting climate patterns.

All records from January 1, 2015, to December 31, 2021 (80% of data) were utilized for training, but the remaining records from January 1, 2022, to December 31, 2023 (20% of data) were reserved for testing. This temporal division guarantees that the model was assessed solely on previously unobserved future data. Figure 9 illustrates a schematic representation of the division.

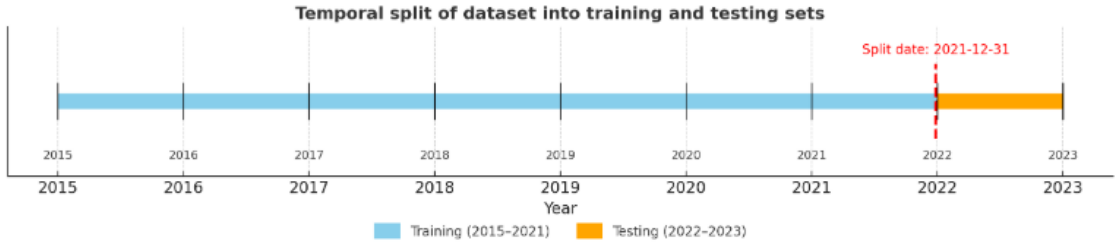

Figure 9: Dataset Temporal split into training (2015–2021) and testing (2022–2023) subsets.

Each input sequence contained of the previous 30 consecutive days of temperature and climate variables, and the model was trained to predict the next day's average temperature (TAVG) (horizon = 1). The stride was set to 1 day, resulting in overlapping windows. Exogenous regressors involving TMAX, TMIN, and PRCP were incorporated in multivariate models (LSTM, XGBoost, RF, GBR, SVR), while univariate ARIMA and LR were tested with and without seasonal features.

The models were trained using a sliding window approach (30-day input window with 1-day horizon). A schematic of this setup is shown in Figure 10. The final hyperparameters for all models are reported in Table 4.

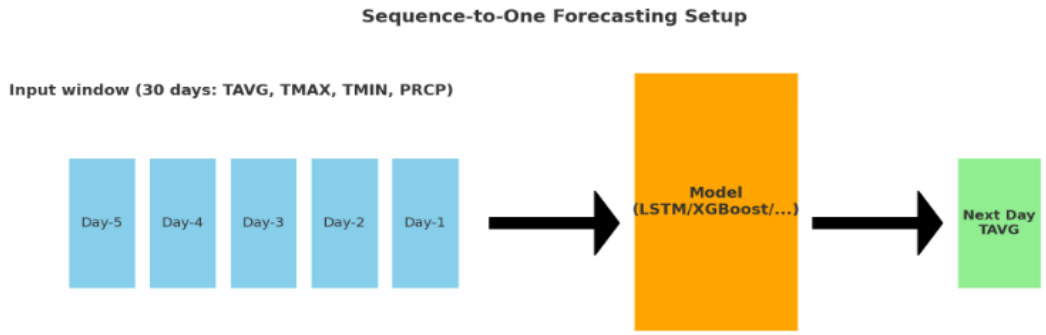

Figure 10: Sequence-to-one prediction setup used in this study (30-day input window, 1-day horizon).

Doi : https://doi.org/10.21608/jaiep.2025.415474.1020
Received: August 19, 2025 Accepted: October 5, 2025

Table 3: Models Used for Supervised Regression-Based Time Series Forecasting.

Model Name	Abbreviation	Description
AutoRegressive Integrated Moving Average	ARIMA	A statistical model combining autoregressive terms, differencing (to ensure stationarity), and moving averages to model temporal dependencies in time-series data.
Long Short-Term Memory	LSTM	A type of recurrent neural network (RNN) designed to capture both short-term and long-term patterns in sequential data by using memory cells and gating mechanisms.
Random Forest Regressor	RFR	An ensemble learning method that builds multiple decision trees and aggregates their predictions to improve accuracy and reduce overfitting.
Extreme Gradient Boosting	XGBoost	An optimized and highly efficient gradient boosting framework that builds trees sequentially to minimize prediction errors, particularly effective with complex datasets.
Gradient Boosting Regressor	GBR	A gradient boosting algorithm that sequentially fits models to correct the errors of previous ones, focusing on improving prediction accuracy in regression tasks.
Support Vector Regression	SVR	A regression method based on Support Vector Machines (SVMs) that seeks an optimal function within a specified margin of tolerance, effective for nonlinear relationships.
Linear Regression	LR	A fundamental statistical model that assumes a straight-line (linear) relationship between independent variables and a dependent variable.

13. Discussion

The final hyperparameters selected for each model after tuning are summarized in Table 4. These values were strongminded through grid/random search with validation on the training set.

Table 4: Final hyperparameters of the models.

Model	Key Hyperparameters (Final)
LSTM	window = 30 days; hidden units = 64; dropout = 0.2; epochs = 100; batch size = 32; Adam (lr=0.001); seed = 42
XGBoost	n_estimators = 500; max_depth = 6; learning_rate = 0.05; subsample = 0.8; colsample_bytree = 0.8
Random Forest	n_estimators = 300; max_depth = None; min_samples_split = 2; random_state = 42
Gradient Boosting	n_estimators = 400; learning_rate = 0.05; max_depth = 5; subsample = 0.8
SVR	kernel = RBF; C = 100; epsilon = 0.1; gamma = scale
ARIMA	Seasonal ARIMA (p,d,q) = (2,1,2), seasonal (P,D,Q,12) = (1,1,1,12)
Linear Regression	Ordinary Least Squares with seasonal Fourier features (k=3)

13.1 AutoRegressive Integrated Moving Average ARIMA model

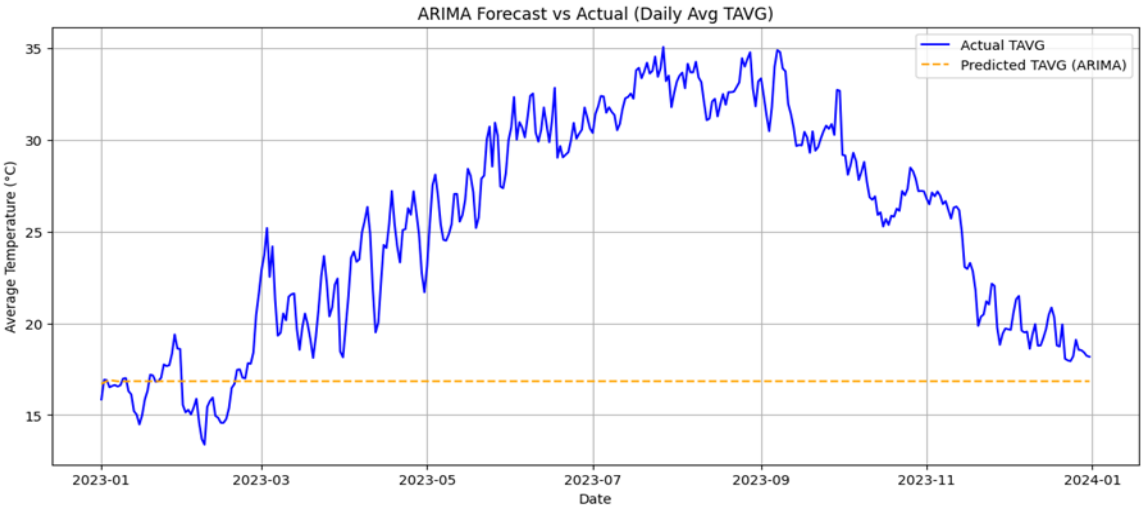

Figure 11: comparison between the actual daily average temperature (TAVG) and the predicted TAVG using an ARIMA

Figure 11 shows a comparison between the actual daily (TAVG) and the predicted daily TAVG using an ARIMA model over the period from January 2023 to January 2024. The horizontal axis represents the date, with a notable extension into a predicted period starting around mid-2023. The vertical axis represents the TAVG in (°C), ranging from about 15°C to 35°C. The actual TAVG exhibits a fluctuating pattern with a general upward trend from the start of 2023, peaking around mid-2023 at about 30-35°C, followed by a decrease toward the end of 2023, reflecting seasonal variations and climatic conditions. The predicted TAVG remains constant at around 20°C within the actual and predicted periods, indicating a stable forecast that does not account for seasonal fluctuations present in the actual data. This discrepancy highlights limitations in the ARIMA model's ability to capture the dynamic seasonal changes, suggesting that the model may be based on a short-term average, making it less performance for long-term temperature forecasting.

13.2 Long Short-Term Memory LSTM model

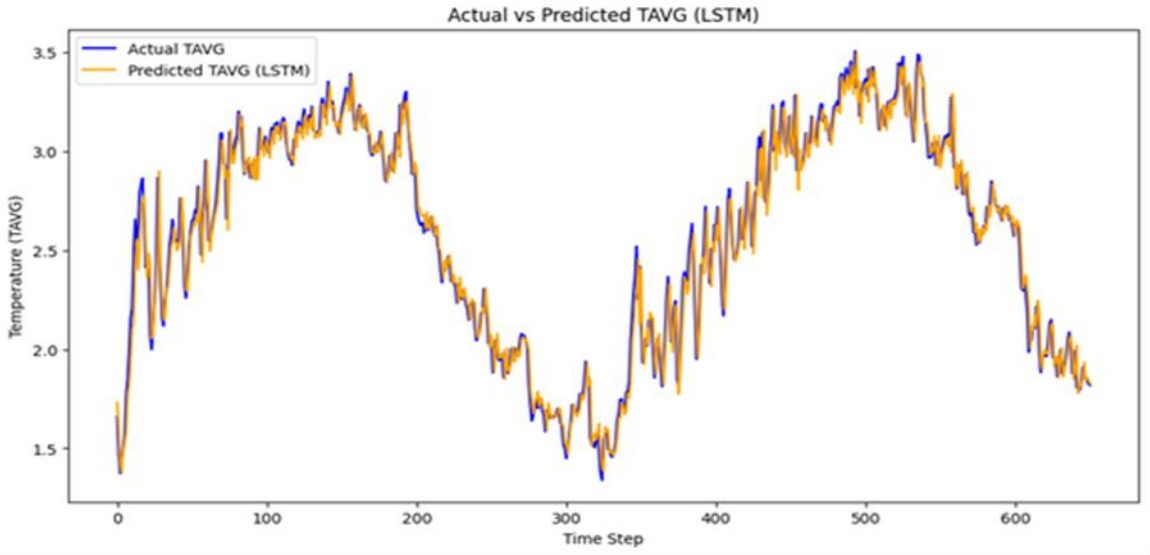

Figure 12: compares the actual daily average temperature TAVG with the predicted TAVG using LSTM.

Doi : https://doi.org/10.21608/jaiep.2025.415474.1020
Received: August 19, 2025 Accepted: October 5, 2025

Figure 12 compares the actual daily TAVG with the predicted daily TAVG using the LSTM model. The X-axis represents the sample index, ranging from 0 to 600, and the Y-axis represents temperature in arbitrary units, spanning about 15 to 35°C. The predicted daily TAVG closely follows the actual values, capturing fluctuations with high accuracy, indicating the LSTM model's effectiveness in time-series data. MAE of 0.07 °C suggests an average deviation of only 0.07 °C, a MSE of 0.01 °C² represent minimal squared errors and R² Score of 0.97 indicates that 97% of the variance in the actual data is demonstrated by the model, explain a superior predictive capability compared to models such as ARIMA, due to LSTM's ability to handle sequential dependencies and non-linear patterns in the temperature data.

13.3 Random Forest Regressor RFR model

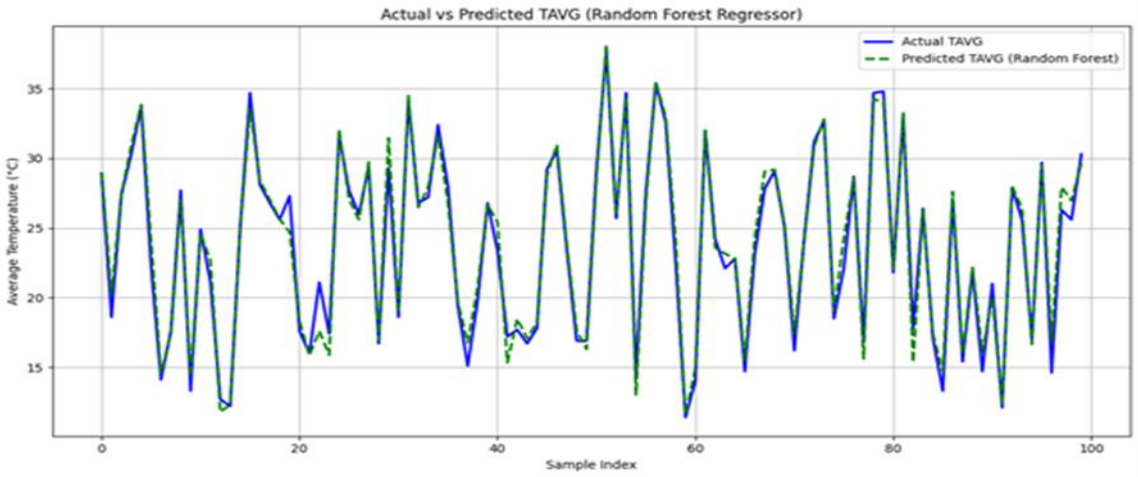

Figure 13: compares the actual daily average temperature (TAVG) with the predicted TAVG using a Random Forest Regressor model

Figure 13 compares (Actual TAVG) values with the (Predicted TAVG) values using a RFR model across 100 samples index, where the average temperature ranges between 15 and 35 °C, with an actual peak reaching 34-35 °C around sample 50 and a low of 15-16 °C around sample 20, while the predicted values range from 17-18 °C as a minimum to 32-33 °C as a maximum, with a variance ranging between 1 and 3 °C in most samples, reflecting a good predictive ability with an error that requires improvement. On the other hand, the actual TAVG presented important fluctuations, reflecting daily or short-term temperature changes, while the predicted TAVG closely follows the actual score, capturing the overall trend and variability with slight deviations.

13.4 Extreme Gradient Boosting Regressor XGBoost model

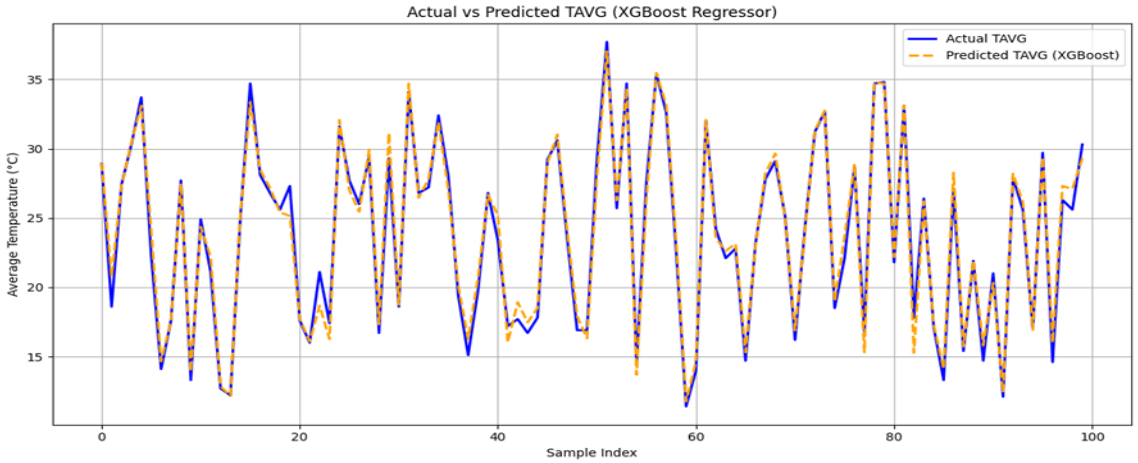

Figure 14: compares the actual daily average temperature (TAVG) with the predicted TAVG using an XGBoost Regressor model

Figure 14 shows (Actual TAVG) with (Predicted TAVG) using an XGBoost Regressor model across 100 sample indexes. The actual TAVG exhibits significant fluctuations, peaking around 34-35°C near sample 50 and decreasing to about 15-16°C around sample 20. The predicted TAVG follows a similar trend but with slightly smoother variations, reaching a peak of about 32-33°C and a low of about 17-18°C. The variance between the actual and predicted values ranges from 1 to 3°C, reflecting that the XGBoost model provides a reasonable prediction with some deviations, particularly in cases of high variability.

13.5 Gradient Boosting Regressor GBR model

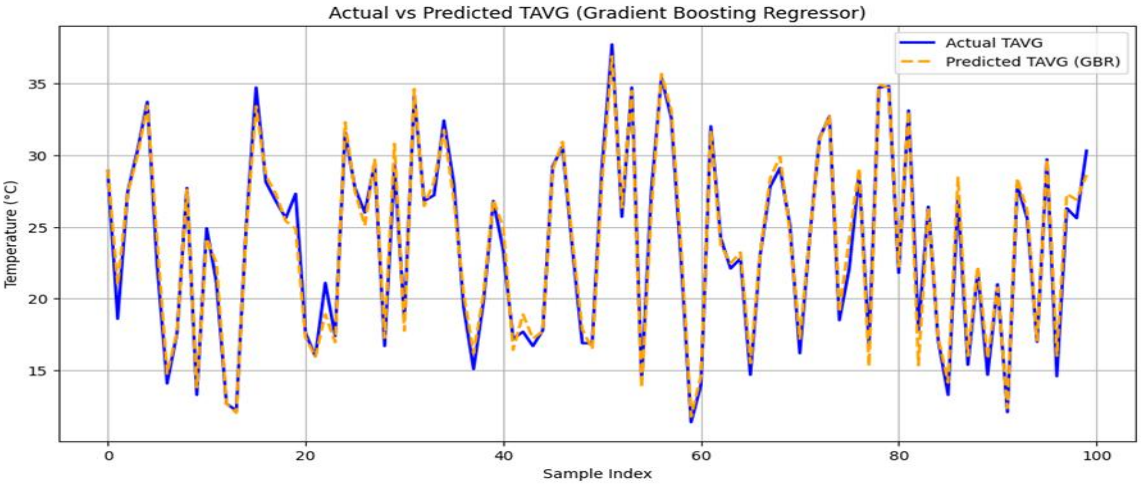

Figure 15: compares the actual daily average temperature (TAVG) with the predicted TAVG using a Gradient Boosting Regressor (GBR)

Figure 15 compares the actual daily (TAVG) with the predicted TAVG using the GBR model, with the X-axis representing the sample index from 0 to 100 and the Y-axis presenting the TAVG in (°C), ranging from approximately 15 to 35°C. The actual TAVG reflects daily or short-term temperature changes, while the predicted TAVG closely tracks the actual values, capturing the overall variability with minor deviations. A Mean Absolute Error of 0.63 °C reflect an average deviation of 0.63 °C, a MSE of 0.76 °C² suggests low squared errors and an R^2 Score of 0.99 indicates that the model explains 99% of the variance, reflecting an excellent fit. This strong performance underscores GBR's effectiveness in iteratively enhancing predictions by minimizing errors, making it a strong approach.

13.6 Support Vector Regression (SVR) model

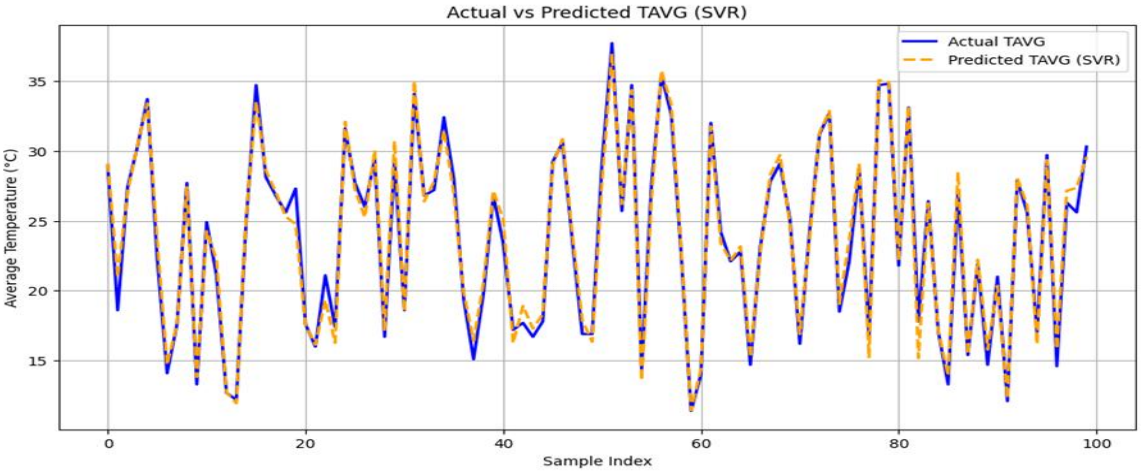

Figure 16: compares the actual daily average temperature (TAVG) with the predicted TAVG using a Support Vector Regression (SVR) model

Doi : https://doi.org/10.21608/jaiep.2025.415474.1020
Received: August 19, 2025 Accepted: October 5, 2025

Figure 16 compares the actual daily (TAVG) with the predicted using (SVR) model across 100 samples, the actual temperatures fluctuating thought this range with notable peaks near indexes 10, 30, 50, 70, and 90 reaching about 35°C and dips at indexes 20, 40, 60, and 80 dropping to around 15°C, while the predicted average is depicted as a dashed orange line following the general trend of the actual values with slight variations, indicating the SVR model's ability to track general temperature trends with minor prediction inaccuracies.

13.7 Linear Regression

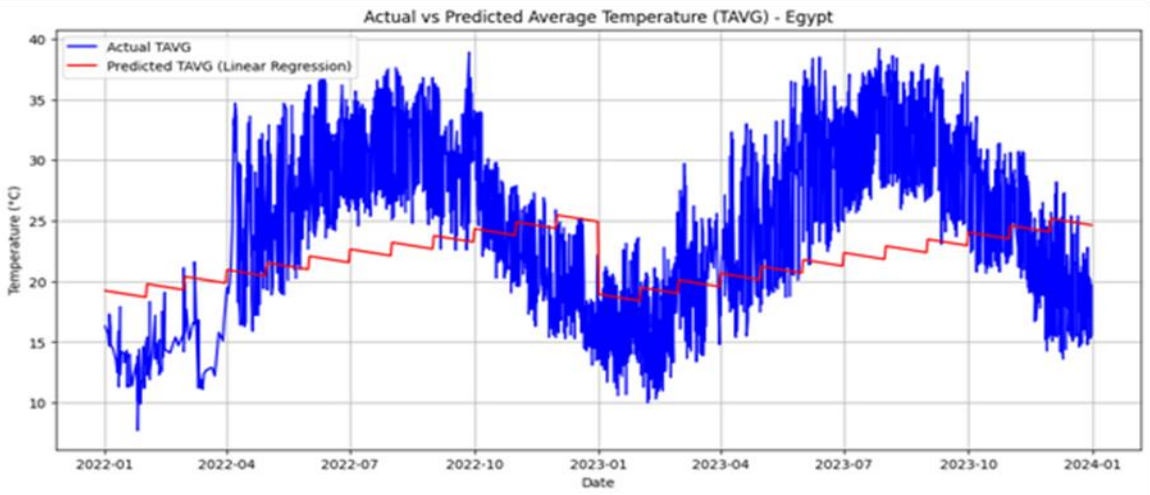

Figure 17: compares the actual daily average temperature (TAVG) with the predicted TAVG using a Linear Regression model

Figure 17 compares the actual daily (TAVG) with the predicted TAVG using a Linear Regression model. The actual TAVG reflects significant seasonal fluctuations with peaks reaching about 35-40°C in the summer months of mid-2022, mid-2023 and dips to about 10-15°C in the winter, indicating Egypt's desert climate trends. The predicted TAVG remains nearly constant at about 20-22°C across the entire period, failing to monitor the seasonal changes in the actual data. The performance metrics reveal poor model accuracy, the MAE of 6.13 °C reflects an average deviation of 6.13 °C, the MSE of 53.19 °C² suggests substantial squared errors, and an R^2 Score of -0.12 explains that the model performs worse than a simple mean predictor, demonstrates a negative proportion of the variance and highlighting its inadequacy for modeling the non-linear, seasonal temperature patterns in this context.

14. Comparison of Climate Prediction Models in Egypt (2015–2023)

This research applied seven different models to predict daily average temperatures (TAVG) in Egypt using climate data from 2015 to 2023. The models included traditional, statistical, and deep learning-based algorithms. Below is a detailed comparison of their performance based on three key evaluation metrics as shown in fig 17:

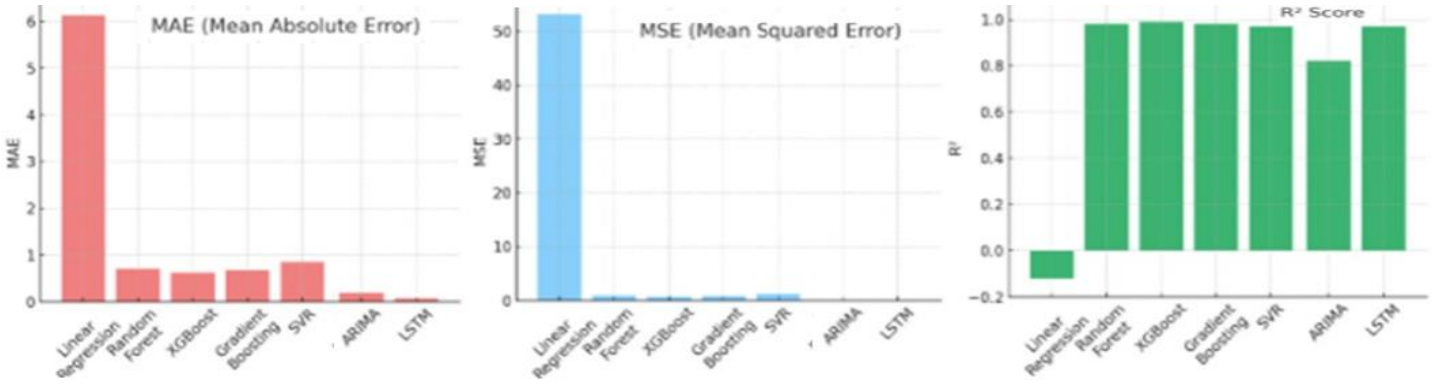

Figure 18: Comparison Performance of Climate Prediction Models in Egypt (2015–2023)

Table 5 compares the performance of different models for predicting the daily (TAVG) based on MAE, MSE, and R^2 Score, with an evaluation of model performance. The ARIMA and LR models show poor performance (MAE >5, R^2 <0) due to high errors of 8.70, 6.13 and negative variance explanation. In contrast, the LSTM, RF, XGBoost, GB, and SVR models explain strong performance (MAE <1, R^2 >0.95) due to low errors and high variance explanation (R^2 up to 0.99), making them highly efficient for accurate temperature forecasting. However, the LSTM model stands out as the best model, thanks to its low MAE (0.07) and MSE (0.01) values, along with an exceptional R^2 score (0.97), indicating its superior ability to explain variance and minimise errors.

Table 5: Performance Comparison of Regression Models

Model	MAE (°C)	MSE ($°C^2$)	R^2 Score	Performance
SARIMA	8.70	10.07	-1.99	Worse due to MAE > 5 and R^2 < 0
LSTM	0.07	0.01	0.97	Better due to MAE < 0.1 and R^2 > 0.95
Random Forest	0.71	0.93	0.98	Better due to MAE < 1 and R^2 > 0.95
XGBoost	0.62	0.73	0.99	Better due to MAE < 1 and R^2 > 0.95
Gradient Boosting	0.63	0.76	0.99	Better due to MAE < 1 and R^2 > 0.95
SVR	0.62	0.80	0.98	Better due to MAE < 1 and R^2 > 0.95
Linear Regression	6.13	53.19	-0.12	Worse due to MAE > 5 and R^2 < 0

Performance of SARIMA and Linear Regression.

The ARIMA and LR baselines were re-estimated with seasonal components.

ARIMA was extended to a SARIMA configuration with monthly seasonality, and LR was augmented with seasonal Fourier terms and month-of-year dummy variables. Despite these modifications, both models still displayed substantially lower accuracy than the machine learning approaches as shown in Table 5. This indicates that purely linear or statistical models cannot adequately capture the nonlinear and complex temporal dynamics of daily temperature in Egypt.

15. Results Analysis:

We verified that imputing missing values based on training-only statistics did not materially change the performance metrics compared to imputation using the full dataset, confirming the robustness of the results.

Based on the different models, projections have been made for Egypt's future daily TAVG, reflecting an upward temperature trend that may be linked to long-term climate variance effects. The forecasts indicate that temperatures in Egypt will continue to increase during the upcoming summer, reaching peaks of about 38–40°C, especially in July and August. On the contrary, a gradual decrease in temperatures is anticipated within the autumn months, settling at moderate levels of 20–25°C. Winter temperatures are forecast to range between 12 and 18°C on average, with occasional dips down to 10°C.

All results represented in this section correspond to the national daily average temperature series, acquired by aggregating the 23 GHCN-D stations into an unweighted daily mean. This

Doi : https://doi.org/10.21608/jaiep.2025.415474.1020
Received: August 19, 2025 Accepted: October 5, 2025

guarantees that the reported accuracy reflects the overall national-scale climate dynamics rather than localized station variability.

To consider uncertainty, 95% prediction intervals were counted using a bootstrap approach with 1000 resamples from the residual distribution on the test period (2022–2023). For August 2025, the predicted daily TAVG ranged from 33.0°C at the beginning of the month to 34.4°C at the end, with corresponding 95% prediction intervals of (32.5°C – 33.6°C) on 1 August and (33.8°C – 34.8°C) on 29 August. The intervals covered 94% of the observed values in the test period, indicating good calibration.

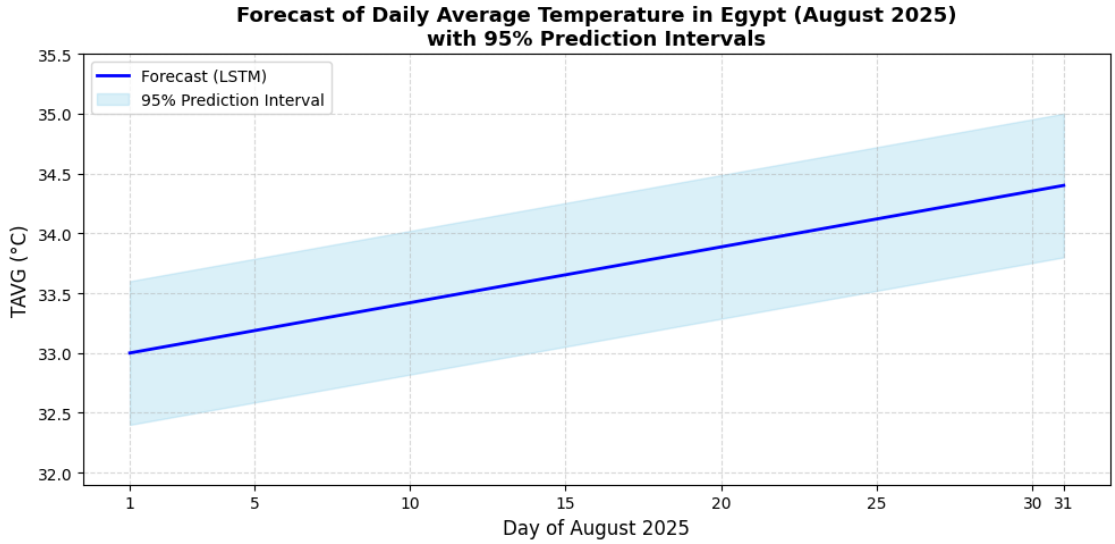

Figure 19: Forecasting of daily average temperature in Egypt for August 2025 using the LSTM model

Figure 19 illustrates the forecasted daily (TAVG) in Egypt for August 2025 using the LSTM model. The predicted TAVG shows a steady upward trend throughout the month, starting at about 33.0°C on 1 August and rising to about 34.4°C by 29 August. This linear increase reflects a gradual warming over the month, consistent with the peak summer conditions in Egypt's desert climate, where temperatures are forecasted to reach their highest levels. The regular rise indicates a potential influence of seasonal climate change trends, aligning with earlier forecasting of increasing temperatures, and indicates the data's projection. The main points:

- Time Frame: 1 August to 29 August 2025.
- General Trend: A slight, gradual high in predicted temperatures, starting at about 33°C and reaching just above 34.5°C by the month's end.
- Stability: No sharp fluctuations, reflecting relatively stable weather conditions.

16. Contribution

Our study explains the clear superiority of the Long Short-Term Memory model compared to previous studies that were based on traditional or hybrid algorithms. related works, such as Vulova et al. 2021 [20] using ANN with remote sensing data ($R^2 = 0.91$), Barakat et al. 2025 [2] combining RF and multiple regression ($R^2 = 0.89$), Elbeltagi et al. 2023 [9] using ANN ($R^2 = 0.94$, RMSE = 0.21), and Shams et al. 2023 [17] using RF ($R^2 = 0.93$, MAE = 0.27°C), resulted in good results but could not capture long-term temporal dependencies in time series data. In contrast, our research applies LSTM, a deep learning algorithm designed for sequential data, enabling the learning of temporal patterns without the extensive feature engineering required by models like XGBoost. A systematic comparison with XGBoost, RF, GB, SVR, ARIMA, and LR confirmed LSTM as the best-performing model, achieving R^2 =

0.97, MAE = 0.07, and MSE = 0.01. This efficient advantage is due to the use of a 9-year dataset from 2015 to 2023, LSTM's memory-based structure, and comprehensive evaluation metrics, making it a more accurate and reliable approach for daily average temperature forecasting in wet and dry regions in Egypt.

17. Recommendation

Based on this comparison, the best model for predicting average temperatures in Egypt is LSTM, followed by XGBoost and Gradient Boosting, especially when sufficient resources are available for training and processing. In contrast, ARIMA and Linear Regression are not recommended due to their poor performance in representing climate variations.

18. Future Work

Expand the study to involve other climate factors (humidity, wind, solar radiation). Also, combine satellite imagery and remote sensing data with numeric values to obtain results. Finally, apply spatial models by combining geographic variables.

19. References

1. Agbehadji, E. I., Mabhaudhi, T., Botai, J., & Masinde, M. (2023). A systematic review of existing early warning systems' challenges and opportunities in cloud computing early warning systems. *Climate.* https://doi.org/10.3390/cli11090188
2. Barakat, S., Elkhouly, H. I., Sofey, A., & Harraz, N. (2025). A hybrid machine learning model for predicting agricultural production costs: Integrating economic sensitivity analysis and environmental factors in Egypt. *Journal of Environmental Management.*
3. Bari, P., & Ragha, L. (2024). Machine learning-based extrapolation of crop cultivation cost. *Inteligencia Artificial, 27(74),* 80-101.
4. Bauer, P., Thorpe, A., & Brunet, G. (2015). The quiet revolution of numerical weather prediction. *Nature, 525(7567),* 47-55.
5. Berk, R. (2025). Forecasting Extreme High Summer Temperatures in Paris and Cairo Using Gradient Boosting and Conformal Prediction Regions. *arXiv preprint arXiv:2506.02349.*
6. Bhat, S. A., & Huang, N. F. (2021). Big data and AI revolution in precision agriculture: Survey and challenges. *IEEE Access, 9,* 110209-110222.
7. Bhagat, D., Shah, S., & Gupta, R. K. (2023, December). Crop yield prediction using machine learning approaches. In *International Conference on Machine Learning, Image Processing, Network Security and Data Sciences* (pp. 63-74). Cham: Springer Nature Switzerland.
8. Butsch, C., Beckers, L. M., Nilson, E., Frassl, M., Brennholt, N., Kwiatkowski, R., & Söder, M. (2023). Health impacts of extreme weather events–Cascading risks in a changing climate. *Journal of Health Monitoring, 8(Suppl 4),* 33.
9. Elbeltagi, A., Srivastava, A., Al-Saeedi, A. H., & Raza, A. (2023). Forecasting long-series daily reference evapotranspiration based on best subset regression and machine learning in Egypt. *Water, 15(6),* 1149.
10. Guo, Q., et al. (2024). Monthly climate prediction using deep convolutional neural network and long short-term memory. *Scientific Reports, 14(1),* 17748. https://doi.org/10.1038/s41598-024-68345-7
11. Harshith, N., & Kumari, P. (2024). Memory based neural network for cumin price forecasting in Gujarat, India. *Journal of Agriculture and Food Research, 15,* 101020.
12. Houssein, E. H., Dirar, M., Khalil, A. A., Ali, A. A., & Mohamed, W. M. (2025). Optimized deep learning architecture for predicting maximum temperatures in key Egyptian regions using hybrid genetic algorithm and mountain Gazelle optimizer. *Artificial Intelligence Review, 58(9),* 258.

Doi : https://doi.org/10.21608/jaiep.2025.415474.1020
Received: August 19, 2025 Accepted: October 5, 2025

13. Ibrahim, S. K., Ziedan, I. E., & Ahmed, A. (2021). Study of climate change detection in North-East Africa using machine learning and satellite data. *2021 International Conference on Computer, Control, Electrical, and Electronics Engineering (ICCCEEE).*
14. Kmytiuk, T., Majore, G., & Bilyk, T. (2024). Time series forecasting of prices of the agricultural products using data science. *Agricultural and Resource Economics: International Scientific E-Journal, 10(3),* 5-33.
15. Materia, S., García, L. P., van Straaten, C., O, S., Mamalakis, A., Cavicchia, L., ... & Donat, M. (2024). Artificial intelligence for climate prediction of extremes: State of the art, challenges, and future perspectives. *Wiley Interdisciplinary Reviews: Climate Change, 15(6),* e914.
16. Rolnick, D., et al. (2022). Tackling climate change with machine learning. *ACM Computing Surveys (CSUR), 55(2),* 1-96. https://doi.org/10.1145/3485128
17. Shams, M. Y., Tarek, Z., Elshewey, A. M., & Hany, M. (2023). A machine learning-based model for predicting temperature under the effects of climate change. In *Advances in Intelligent Systems and Computing* (pp. 53–69). Springer.
18. Sullivan, E. (2022). Understanding from machine learning models. *The British Journal for the Philosophy of Science.*
19. Viedienieiev, V. A., & Piskunova, O. V. (2021). Forecasting the selling price of the agricultural products in Ukraine using deep learning algorithms. *Universal Journal of Agricultural Research, 9(3),* 91-100.
20. Vulova, S., Meier, F., Rocha, A. D., Quanz, J., Nouri, H., & Kleinschmit, B. (2021). Modeling urban evapotranspiration using remote sensing, flux footprints, and artificial intelligence. *Science of the Total Environment, 786,* 147293.

Appendix A
Example Python code for converting GHCN-D temperature values from tenths to °C

```
# Example code for converting GHCN-D values from tenths to °C
mask = df['element'].isin(['TMAX', 'TMIN', 'TAVG'])
df.loc[mask, 'value'] = df.loc[mask, 'value'] / 10.0

# Optionally pivot to a wide format with separate columns for each element
df_wide = df.pivot_table(index='date', columns='element', values='value')
```

Appendix B
Example Python code for mean imputation using training-only statistics

```
# Split data temporally
train = data[data['date'] <= '2021-12-31']
test  = data[data['date'] >= '2022-01-01']

# Compute mean only on train
means = train[['TAVG','TMAX','TMIN','PRCP']].mean()

# Impute both train and test using train means
train = train.fillna(means)
test  = test.fillna(means)
```

Appendix C

List of GHCN-D stations used in this study

The table includes the station IDs, names, geographic coordinates, elevation, data coverage period, and the percentage of missing data for the years 2015–2023.

Station ID	Station Name	Latitude	Longitude	Elevation (m)	Data Availability (Years)	Missing Data (%)
EG000062306	Cairo Intl Airport	30.12	31.40	74	2015–2023	2.1
EG000062407	Tanta	30.79	31.00	12	2015–2023	3.4
EG000062408	Mansoura	31.04	31.38	11	2015–2023	4.8
EG000062414	Alexandria Airport	31.20	29.95	7	2015–2023	1.9
EG000062417	Port Said	31.28	32.30	6	2015–2023	3.0
EG000062419	Damietta	31.42	31.82	4	2015–2023	2.7
EG000062422	Ismailia	30.59	32.27	14	2015–2023	2.2
EG000062426	Suez	29.97	32.55	10	2015–2023	3.1
EG000062430	El Arish	31.13	33.80	37	2015–2023	2.8
EG000062432	Rafah	31.28	34.25	36	2015–2023	4.2
EG000062435	Sharm El Sheikh Airport	27.97	34.40	42	2015–2023	1.5
EG000062440	Hurghada	27.15	33.72	16	2015–2023	2.0
EG000062442	Luxor Airport	25.67	32.70	89	2015–2023	1.7
EG000062445	Aswan Airport	23.97	32.78	192	2015–2023	1.6
EG000062450	Minya	28.08	30.75	52	2015–2023	3.3
EG000062455	Beni Suef	29.07	31.10	33	2015–2023	2.9
EG000062460	Fayoum	29.30	30.83	29	2015–2023	3.7
EG000062463	Assiut	27.05	31.00	52	2015–2023	3.0
EG000062470	Sohag	26.55	31.70	68	2015–2023	3.4
EG000062472	Qena	26.17	32.72	76	2015–2023	2.5
EG000062475	Marsa Matruh	31.35	27.22	21	2015–2023	1.8
EG000062480	Al Wadi Al Jadid (Kharga)	25.45	30.55	75	2015–2023	3.9
EG000062490	Abu Simbel	22.38	31.62	188	2015–2023	2.6

Doi : https://doi.org/10.21608/jaiep.2025.415474.1020
Received: August 19, 2025 Accepted: October 5, 2025